altered $\nu(Fe^{II}—O_2)$ value reported for HRP-III may be attributable to some other type of distal perturbation.

For insight into the nature of this perturbation, we consider the function, in particular the initial reaction steps, of a peroxidase. The peroxidase heme pocket binds hydrogen peroxide in a manner that facilitates the cleavage of the O—O bond. This is most likely accomplished by the action of a positively charged arginine group that pulls electron density out of the O—O bond of the peroxide.[70e] Removal of electron density from the O=O bond of dioxygen, however, *strengthens* the bond because the HOMO is antibonding. Thus, when O_2 rather than HOOH is bound in the peroxide heme crevice, the oxygen-oxygen bond is strengthened and $\nu(O=O)$ increases while $\nu(Fe^{II}—O_2)$ decreases. These distal effects on the electron density in the O=O bond of the bound dioxygen presumably overshadow the trans-ligand effects of the proximal histidine and thus explain the $\nu(Fe^{II}—O_2)$ frequency of HRP-III. On the other hand, in an oxidase, cleavage of the dioxygen bond is likely accomplished by adding electron density into the O=O bond, as this further populates the π^* orbital. Thus, in cytochrome oxidase intermediates, the dioxygen may assume a configuration that tends to build electron density between the oxygen atoms, resulting in a decrease in the $\nu(O=O)$ frequency and a concomitant increase in the $\nu(Fe^{II}—O_2)$ frequency. Our time-resolved studies, however, show that the initial Cyt Ox $a_3—O_2$ complex is relatively unperturbed by distal effects.[3] Thus, weakening and rupture of the O=O bond occurs in a subsequent step of the reaction.

Acknowledgment. We thank Dr. B. Ward, Professors J. R. Kincaid and J. Terner, and especially Professor C. K. Chang for valuable discussions. We thank Professors J. S. Olson and J. Terner for manuscripts prior to publication and Professor R. J. Mardon for travel assistance. Dr. Hans Hoogland is acknowledged for preparing the myeloperoxidase samples. We are especially grateful to Professor L. Andersson for critical evaluation of our manuscript and for several manuscripts prior to publication. This work was supported by grants from the Netherlands Organization for the Advancement of Pure Research (ZWO) under the auspices of the Netherlands Foundation for Chemical Research (SON) to R.W. and from the U.S. National Institutes of Health (GM 25480) to G.T.B. R.W. acknowledges the receipt of a travel grant from the Netherlands Organization for the Advancement of Pure Research (ZWO). This collaboration was made possible by a NATO Research Grant (No. 86/734).

Contribution from the Department of Chemistry,
Texas A&M University, College Station, Texas 77843-3255

Redox Chemistry of Iron Picolinate Complexes and of Their Hydrogen Peroxide and Dioxygen Adducts

Pablo Cofré, Silvia A. Richert, Andrzej Sobkowiak, and Donald T. Sawyer*

Received May 31, 1989

In aprotic solvents the bis(picolinato)iron(II) [$Fe(PA)_2$] and (2,6-pyridinedicarboxylato)iron(II) [Fe(DPA)] complexes react with hydrogen peroxide and with dioxygen to form a series of monooxygen and dioxygen intermediates and adducts [$(PA)_2FeOFe(PA)_2$ (**1**), $(PA)_2Fe(OO)$, $(PA)_2FeOFe(PA)_2$·HOOH (**2**), and their analogues with Fe(DPA)]. The electron-transfer chemistries of the complexes and of their oxygenated products have been characterized by cyclic voltammetry, controlled-potential electrolysis, and rotated ring-disk voltammetry. These results in combination with UV-visible spectrophotometric and magnetic measurements have been used to develop a self-consistent mechanism for the formation of $(PA)_2FeO(OO)Fe(PA)_2$ (**3**) from $(PA)_2FeOFe(PA)_2$ (**1**) and HOOH and for its transformation of methylene carbons to ketones. In dimethylformamide, species **3** (formed from **1** and HOOH) spontaneously decomposes to singlet dioxygen ($^1O_2$) and **1**.

The electron-transfer chemistry of transition-metal complexes in aprotic solvents has been of major interest for the past two decades, especially in relation to oxygen activation by metalloproteins. Because iron is the most common metal in such metalloenzymes, its mode of activation for HOOH and for O_2 via redox cycles of various iron complexes can provide insight into the catalytic mechanisms of oxidases, peroxidases, monooxygenases, and dioxygenases. The coordination complexes of iron(III) are prone to form μ-oxo-bridged dimers.[1-3] The mononuclear 8-quinolinol and 2-methyl-8-quinolinol complexes of iron(II) and -(III) react with molecular oxygen and hydrogen peroxide to form such μ-oxo dimers, which are catalytic for the decomposition of the superoxide ion.[4]

Related studies of manganese complexes as reaction mimics for the water oxidation cofactor in photosystem II indicate that the picolinate[5,6] and 2,6-pyridinedicarboxylate[7] ligands form especially rugged and relevant models for the manganese cofactor. When these ligands are coordinated to manganese, cobalt, and iron, they exhibit ligand-centered redox processes with redox potentials of +0.6 to -0.0 V vs NHE for the ML_3/ML_3^- process.[7,8] The tris(picolinato)manganese(III) complex facilitates the decomposition of hydrogen peroxide,[5] and the tris(picolinato)manganese(II) complex $Mn(PA)_2(PAH)(H_2O)$ efficiently catalyzes the disproportionation of superoxide ion in acetonitrile or dimethyl sulfoxide[9] [as does the bis(8-quinolinolato)manganese(II) complex].[10] In aqueous media tris(picolinato)iron(II) catalyzes the decomposition of the superoxide ion via the generation of hydrogen peroxide and its iron-induced activation to produce hydroxyl radicals.[11]

(1) Ehman, D. L.; Sawyer, D. T. *Inorg. Chem.* **1969**, *8*, 900.
(2) Wilkins, R. G.; Yelin, R. E. *Inorg. Chem.* **1969**, *8*, 1470.
(3) Schugar, H. J.; Hubbard, A. T.; Anson, F. C.; Gray, H. B. *J. Am. Chem. Soc.* **1969**, *91*, 71.
(4) Seo, E. T.; Riechel, T. L.; Sawyer, D. T. *Inorg. Chem.* **1977**, *16*, 734.
(5) Yamaguchi, K.; Sawyer, D. T. *Inorg. Chem.* **1985**, *24*, 971.
(6) Matsushita, T.; Spencer, L.; Sawyer, D. T. *Inorg. Chem.* **1988**, *27*, 1167.
(7) Richert, S. A.; Tsang, P. K. S.; Sawyer, D. T. *Inorg. Chem.* **1988**, *27*, 1814.
(8) Richert, S. A.; Tsang, P. K. S.; Sawyer, D. T. *Inorg. Chem.* **1989**, *28*, 2471.
(9) Yamaguchi, K. S.; Spencer, L.; Sawyer, D. T. *FEBS Lett.* **1986**, *197*, 249.
(10) Howie, J. K.; Sawyer, D. T. *J. Am. Chem. Soc.* **1976**, *98*, 6698.
(11) Bannister, W. H.; Bannister, J. V.; Searle, A. J. F.; Thornalley, P. J. *Inorg. Chim. Acta* **1983**, *78*, 139.

0020-1669/90/1329-2645$02.50/0

The present study has been directed to the electron-transfer reactions of the picolinate (PA) and 2,6-pyridinedicarboxylate (DPA) complexes of iron and their adducts with molecular oxygen and hydrogen peroxide in dimethylformamide and pyridine/acetic acid solvents. Recent studies[12] have shown that $Fe(PA)_2$ and $(PA)_2FeOFe(PA)_2$ activate HOOH [and KO_2(s) or electroreduced O_2] in a pyridine/acetic acid solvent system for the efficient and selective transformation of methylene carbons to ketones and for the dioxygenation of acetylenes and aryl olefins. In the same solvent matrix the combination of $Fe(PA)_2$, HOOH, PhSeSePh, and a hydrocarbon substrate (e.g., c-C_6H_{12}) (2:2:1:100 mole ratio) in py/HOAc reacts stoichiometrically to give 2 equiv of the PhSe derivative of the substrate [e.g., 2-(c-C_6H_{11})SePh].[13] In the presence of O_2 (1 atm, 3.4 mM) and excess substrate, the $Fe^{II}(DPAH)_2$ complex is autoxidized to a reactive intermediate, which ketonizes methylene carbons and dioxygenates acetylenes, aryl olefins, and catechols.[14]

Experimental Section

Equipment. A three-electrode potentiostat (Bioanalytical Systems Model CV-27) with a Houston Instruments Model 200 XY recorder was used to record the voltammograms. The experiments were conducted in a 15-mL electrochemical cell with provision to control the presence of oxygen with an argon-purge system. The working electrode was a Bioanalytical Systems glassy-carbon inlay (area 0.09 cm^2), the auxiliary electrode was a platinum wire, and the reference electrode was a Ag/AgCl wire in an aqueous tetramethylammonium chloride solution that was adjusted to give a potential of 0.00 V vs SCE. The last was contained in a Pyrex tube with a cracked soft-glass tip, which was placed inside a luggin capillary.[15]

Controlled-potential electrolyses were performed wiih a three-electrode potentiostat (Princeton Applied Research Model 173 potentiostat/galvanostat, Model 175 universal programmer, and Model 179 digital coulometer). The same microcell assemblies and Ag/AgCl reference electrodes as those employed for cyclic voltammetry were used. The working electrode was a glassy-carbon plate, and the auxiliary electrode was a platinum flag. The reaction products were separated and identified with a Hewlett-Packard Model 5880A gas chromatograph equipped with a HP-1 capillary column (cross-linked methylsilicone gum phase, 12 m × 0.2 mm).

The rotated ring–disk measurements were made with a Pine Instruments Co. Model PIR rotator with a GC–GC ring–disk electrode. The parameters of the electrode were r_1 = 0.382 cm, r_2 = 0.416 cm, r_3 = 0.556 cm, and N = 0.418. Potential control was provided by a Pine Instruments Co. Model RDE 3 dual potentiostat. The sample solutions and electrode assembly (including a Pt auxiliary electrode and a Ag/AgCl reference electrode in a luggin capillary) were contained in a 150-mL beaker with a Leeds and Northrup plastic cell top. The ring currents and disk currents vs disk potential in the collection-efficiency experiments were recorded simultaneously on two Houston Instruments Model 2000 XY recorders. A Hewlett-Packard Model 8450A diode-array spectrophotometer was used for the UV–visible measurements. Fast-kinetics experiments were performed with a Tractor Northern Model SF-1000 stopped-flow spectrophotometer that was equipped with a Model TN-6500 rapid-scan spectrometer. Magnetic susceptibility measurements were made with a Johnson Matthey Chemicals Ltd. Model MSB1 magnetic susceptibility balance.

Reagents. The chemicals and solvents for the investigations and syntheses were of the highest purity available and were used without further purification: acetonitrile (MeCN), dimethylformamide (DMF), and pyridine (py) from Burdick and Jackson ("distilled in glass" grade); methanol (MeOH) and acetic acid (HOAc) from J. T. Baker ("Baker analyzed" grade); tetraethylammonium perchlorate (TEAP, vacuum-dried for 24 h prior to use) and ferrous perchlorate [$Fe(ClO_4)_2 \cdot 6H_2O$] from GFS Chemcials; ferric perchlorate [$Fe(ClO_4)_3$] from Strem Chemicals, Inc.; Picolinic acid (PAH), 2,6-pyridinedicarboxylic acid ($DPAH_2$), cyclohexane, and 1,4-cyclohexadiene (1,4-CHD) from Aldrich Chemical Co., Inc.; tetramethylammonium hydroxide [$(Me_4N)OH$, 25% w/w solution in methanol from Aldrich (its concentration was determined by acid–base titration) or the pentahydrate solid from Fluka Chemika].

Hydrogen peroxide (50% from Fisher Scientific) was used as the starting material for the preparation of anhydrous HOOH,[16] which was diluted in MeCN to make a 3.5 M stock solution. The concentration of HOOH was determined by iodometric titrations. Tetramethylammonium picolinate [$(Me_4N)PA$] and tetramethylammonium dipicolinates [$(Me_4N)_2DPA$ and $(Me_4N)HDPA$] were prepared by crystallization from MeCN of a stoichiometric combination of PAH (and $DPAH_2$) and $(Me_4N)OH$. $(Me_4N)_2DPA$ and $(Me_4N)HDPA$ were recrystallized from a 95% MeCN/5% MeOH mixture, and the dried product was assayed by acid–base titration. A $[Fe(MeCN)_4](ClO_4)_2$ stock solution in MeCN was made from the recrystallized salt. Stock solutions of $(Me_4N)PA$ in MeCN and of $(Me_4N)_2DPA$ and $(Me_4N)HDPA$ in MeCN/MeOH were used for the various experiments, and $Fe(ClO_4)_3$ was dissolved in MeCN.

$(PA)_2FeOFe(PA)_2$. Addition of 1 equiv of HOOH to 2 equiv of $Fe(PA)_2$ in MeCN (20 mM, orange solution) gave an immediate discoloration and the formation of a pale green precipitate, which was separated by filtration, recrystallized from a MeCN/MeOH mixture, and dried on a vacuum line. The pale green powder, $[(PA)_2Fe(OH)]_2$ (**1a**), dissolved in DMF to give a strong absorption maximum [λ_{max} 350 nm (ϵ 3100 cm^{-1} M^{-1})] and an irreversible reduction at −0.65 V vs SCE; in py/HOAc (2:1 mole ratio) the absorption maximum was at 350 nm (ϵ 2260 cm^{-1} M^{-1}). The isolated solid had infrared bands at 694, 708, 760, 857, 1020, and 1047 cm^{-1} and a magnetic moment of 7.0 ± 0.5 μ_B per dimer (or 4.9 μ_B per Fe). In DMF, **1a** had a magnetic moment (Evans' method) of 3.6 ± 0.3 μ_B per dimer (2.5 μ_B per Fe). The elemental analysis of the pale green powder, $[(PA)_2Fe(OH)]_2$ (**1a**), was performed by Galbraith Laboratories, Inc. Anal. Calcd for $C_{24}H_{18}N_4O_{10}Fe_2$: C, 45.46; H, 2.86; N, 8.84; O, 25.23; Fe, 17.61. Found: C, 45.17; H, 3.08; N, 8.80; O, 25.31; Fe, 16.93.

The 1:1 combination of $Fe(PA)_3$ and $(Me_4N)OH \cdot 5H_2O$ in DMF gave a golden brown solution of a product species, $(PA)_2FeOFe(PA)_2$ (**1b**), with a magnetic moment of 3.1 ± 0.2 μ_B per dimer (2.2 μ_B per Fe), an irreversible reduction at −0.85 V vs SCE, and a strong UV absorption band [λ_{max} 350 nm (ϵ 3300 cm^{-1} M^{-1})].

Results

Electrochemistry of the Fe^{II}/PA and Fe^{II}/DPA Systems. Figure 1 illustrates the cyclic voltammograms for various combinations of $[Fe(MeCN)_4](ClO_4)$ with $(Me_4N)PA$ and $(Me_4N)_2DPA$ in dimethylformamide (DMF). The 1:3 (Fe^{II}:PA) and 1:2 (Fe^{II}:DPA) combinations exhibit cleanly reversible voltammograms that are characteristic of a single oxidized complex in each case [$Fe(PA)_3$ and $Fe(DPA)_2^-$]. The results also confirm that the $Fe(PA)_2$ and Fe(DPA) complexes are formed. The addition of excess ligand (>3:1 for PA^- and >2:1 for DPA^{2-}) results in oxidation peaks for the free ligand (PA^-, +1.25 V vs SCE; DPA^{2-}, +1.11 and +1.33 V vs SCE). The redox reactions for these complexes and their electron-transfer potentials are summarized in Table I.

Reactivity of HOOH and O_2. (a) Electrochemical Measurements. The cyclic voltammograms for the product species from the addition of HOOH to $Fe^{II}(PA)_2$ and Fe^{II}(DPA) are presented in Figure 1. For $Fe(PA)_2$ the rest potential at −0.14 V vs SCE (prior to HOOH addition) is shifted to +0.08 V, and the anodic peak for an initial positive voltage scan is completely eliminated and replaced by two new irreversible reduction peaks (−0.65 V vs SCE and −0.85 V). For Fe(DPA) the rest potential shifts from −0.27 to +0.15 V, and its oxidation peaks are replaced by a new reversible reduction couple (−0.34/−0.20 V). The broad adsorption band for $Fe^{II}(PA)_2$ [λ_{max} 462 nm (ϵ 1200 cm^{-1} M^{-1})] is replaced by a large absorption edge that rises abruptly below 400 nm [λ 350 nm (ϵ 3300 cm^{-1} M^{-1})] upon the stoichiometric addition of HOOH. Fe(DPA) exhibits similar behavior with the absorption for the parent compound [λ_{max} 484 nm (ϵ 620 cm^{-1} M^{-1})] replaced by a strong UV absorption band [λ 350 nm (ϵ 3100 cm^{-1} M^{-1})].

Addition of dioxygen (O_2, 1 atm and 4.8 mM) to a solution that contains $Fe(PA)_2$ causes a positive shift of the rest potential and a gradual elimination of the anodic peak for $Fe(PA)_2$ (Figure 2). After 64 h an initial negative scan yields the same reduction peaks that result from the combination of $Fe(PA)_2$ and HOOH (Figure 1A).

In contrast, addition of O_2 to Fe(DPA) results in the almost instantaneous transformation to a single oxidized product with

(12) Sheu, C.; Richert, S. A.; Cofrê, P.; Ross, B., Jr.; Sobkowiak, A.; Sawyer, D. T.; Kanofsky, J. R. *J. Am. Chem. Soc.* **1990**, *112*, 1936.
(13) Sheu, C.; Sobkowiak, A.; Zhang, D.; Ozbalik, N.; Barton, D. H. R.; Sawyer, D. T. *J. Am. Chem. Soc.* **1989**, *111*, 8030.
(14) Sheu, C.; Sobkowiak, A.; Jeon, S.; Sawyer, D. T. *J. Am. Chem. Soc.* **1990**, *112*, 879.
(15) Sawyer, D. T.; Roberts, J. L., Jr. *Experimental Electrochemistry for Chemists*; Wiley-Interscience: New York, 1974; p 144.
(16) Brauer, G. *Handbook of Preparative Inorganic Chemistry*; Academic Press: New York, 1963; pp 140–142.

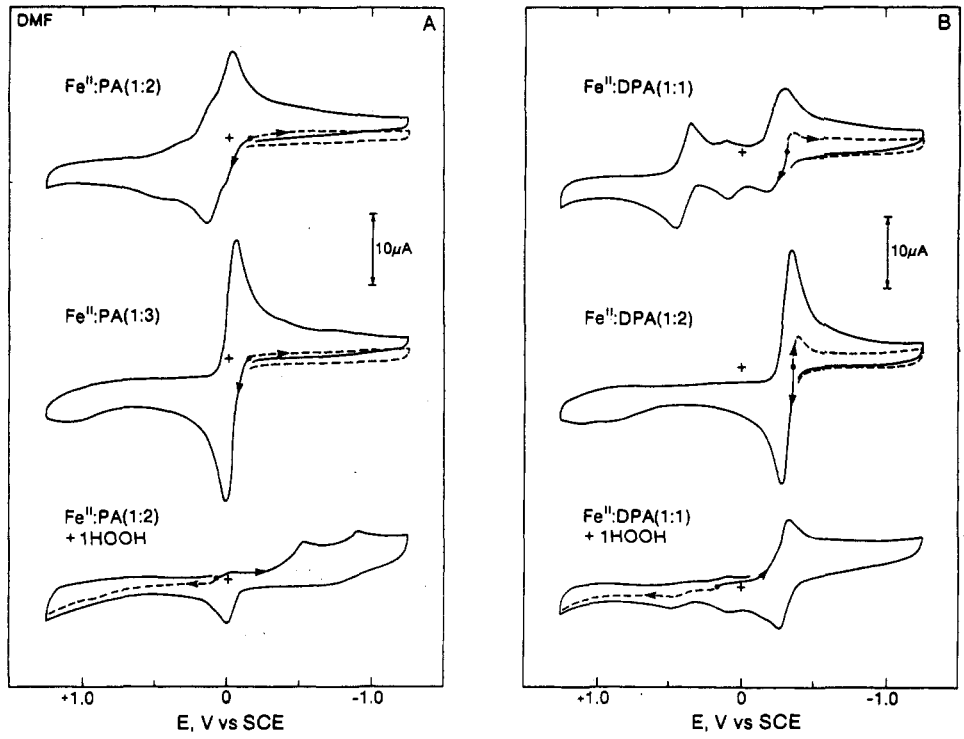

Figure 1. Cyclic voltammograms in DMF (0.1 M TEAP) of (A) 2 mM Fe^{II}/PA (1:2 and 1:3) and 2 mM Fe^{II}/PA (1:2) + 1 equiv of HOOH and (B) 2 mM Fe^{II}/DPA (1:1 and 1:2) and 2 mM Fe^{II}/DPA (1:1) + 1 equiv of HOOH [scan rate 0.1 V s^{-1}; GCE (area 0.09 cm^2)].

Table I. Redox Reactions and Electrochemical Potentials for Iron Picolinate (PA) and Iron Dipicolinate (DPA) Complexes in DMF and py/HOAc (2:1 Mole Ratio)

redox couple	$E_{1/2}$ (or E_p), V vs SCE
A. DMF Solvent	
$Fe(PA)_3^- \rightleftarrows Fe(PA)_3 + e^-$	−0.03
$Fe(PA)_2 + H_2O \overset{DMF}{\rightleftharpoons} (PA)_2Fe(OH) + H(DMF)^+ + e^-$	+0.10
$Fe(DPA)_2^{2-} \rightleftarrows Fe(DPA)_2^- + e^-$	−0.31
$Fe(DPA) + H_2O \overset{DMF}{\rightleftharpoons} (DPA)Fe(OH) + H(DMF)^+ + e^-$	+0.11
$Fe(DMF)_n^{2+} \rightleftarrows Fe(DMF)_n^{3+} + e^-$	+0.41
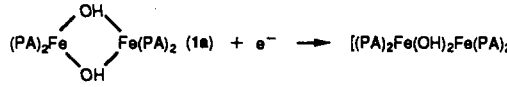	−0.65
$(PA)_2FeO(PA)_2$ (**1b**) $+ e^- \rightarrow [(PA)_2FeOFe(PA)_2]^-$	−0.85
$(DPA)FeOFe(DPA) + e^- \rightleftarrows [(DPA)FeOFe(DPA)]^-$	−0.31
$Fe(DPA)^+ + e^- \rightleftarrows Fe(DPA)$	+0.15
$(DPA)FeOO^{\bullet} + e^- \rightarrow (DPA)FeOO^-$	+0.4
B. py/HOAc Solvent (2:1 Mole Ratio)	
$HOOH \xrightarrow{py} O_2 + 2Hpy^+ + 2e^-$	+1.25
$(PA)_2FeOFe(PA)_2 \xrightarrow[(HOOH)]{py} O_2 + 2Hpy^+ + (PA)_2FeOFe(PA)_2 + 2e^-$	+1.00
$(DPA)_2FeOFe(DPA)_2 \xrightarrow[(HOOH)]{py} O_2 + 2Hpy^+ + (DPA)_2FeOFe(DPA) + 2e^-$	+1.00

a reversible redox couple (Figure 2B) (the red-brown color of Fe(DPA) is bleached to almost colorless). The electrochemistry of the product solution is the same as that for the product from the combination of Fe(DPA) and HOOH (Figure 1B).

Figure 3 illustrates the cyclic voltammograms in pyridine/acetic acid (2:1 mole ratio) of an isolated $Fe(PA)_2$ salt that has been exposed to atmospheric oxygen for 1 year ["$Fe(PA)_2$"]. In DMF this material has electrochemistry that is identical with that for a solution of $Fe(PA)_2$ that has been exposed to O_2 for 30 min (Figure 2B). The effects of the addition of 0.5 and 2.0 equiv of HOOH/equiv of "$Fe(PA)_2$" are indicated by curves b and c of Figure 3; curve d indicates the changes in the latter solution after 23 h.

The isolated product from the combination of 2 equiv of $(PA)_2Fe$ with 1 equiv of HOOH in MeCN is a pale greenish white material that has an intense absorption band at λ 350 nm (ε 2260 cm^{-1} M^{-1}) and electrochemistry in DMF that is identical with that of the bottom cyclic voltammogram of Figure 1A. The isolated complex has a magnetic moment of 4.9 μ_B per iron and an elemental analysis that is consistent with a binuclear formulation for the complex $[(PA)_2Fe(OH)]_2$ (**1a**) or $[(PA)_2FeOFe(PA)_2 \cdot H_2O]$ (**1b**).

The results from the addition of excess HOOH to $Fe(PA)_2$ and Fe(DPA) in DMF and in pyridine/acetic acid (2:1 mol ratio) are illustrated by the cyclic voltammograms of Figure 4. In DMF a rapid decomposition of HOOH occurs with gas evolution

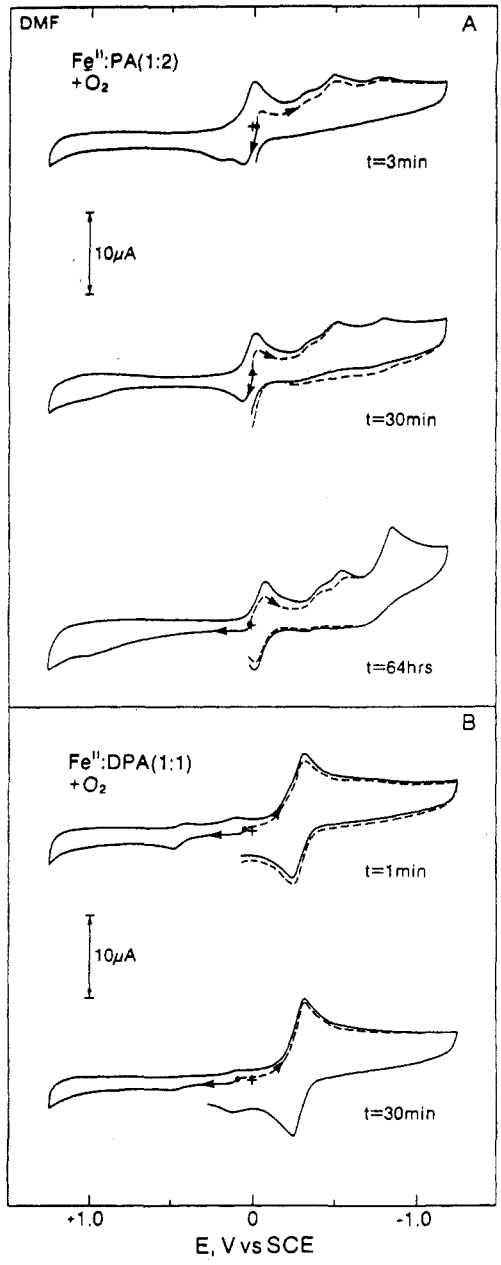

Figure 2. Cyclic voltammograms as function of time in DMF (0.1 M TEAP) of (A) 2 mM Fe^{II}/PA (1:2) + O_2 (1 atm) and (B) 2 mM Fe^{II}/DPA (1:1) + O_2 (1 atm) [scan rate 0.1 V s^{-1}; GCE (area 0.09 cm^2)].

[complete in 30 min with $Fe(PA)_2$ and in 15 min with Fe(DPA)]. With continuous purging of the solutions and after completion of the reaction, the solutions exhibit cyclic voltammograms that are the same as those for the 1:1 combinations of $Fe(PA)_2$/HOOH and Fe(DPA)/HOOH (Figure 1). Further additions of HOOH to these product solutions result in the same catalytic cycles.

The cyclic voltammograms of Figure 4A result from a continuously cycled electrode in a solution to which HOOH is added at the indicated points (Figure 1 illustrates cyclic voltammograms in the absence of HOOH). Further cycling shows a decay with time of the −0.85−V reduction peak, which disappears completely upon completion of the decomposition reaction. Addition of O_2 causes the −0.85-V reduction to increase.

When HOOH is added to $Fe(PA)_2$ and Fe(DPA) in py/HOAc (2:1 mole ratio), there is no evolution of gas and the cyclic voltammograms for the resulting solutions (after 15 min) exhibit two new oxidation peaks at +1.0 and +1.25 V vs SCE (the latter is the same as that for free HOOH in this solvent). Figure 4 illustrates these voltammograms, which do not change over a 72-h period.

The cyclic voltammogram of 3.5 mM $Fe(PA)_2$ in py/HOAc

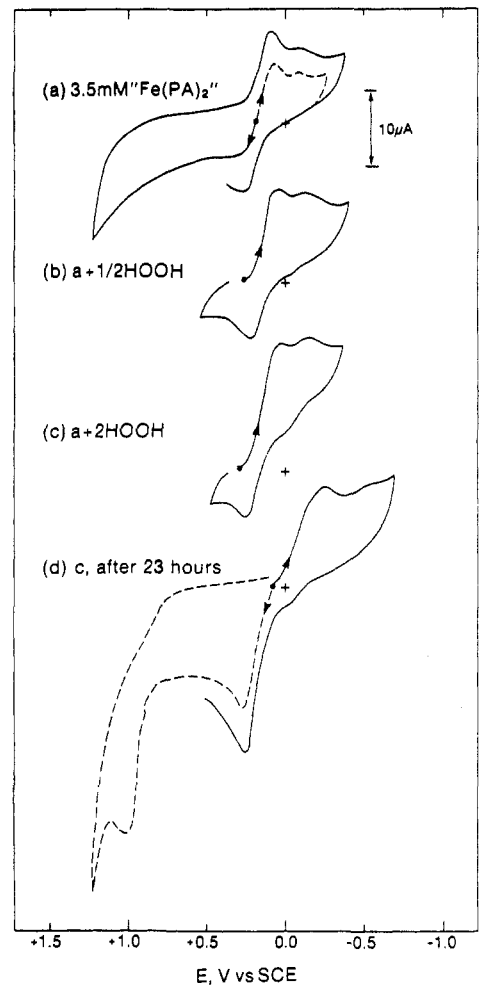

Figure 3. Cyclic voltammograms of (a) 3.5 mM "$Fe(PA)_2$" [air-oxidized $Fe(PA)_2$] in 2:1 py/HOAc (0.1 M TEAP), (b) 3.5 mM "$Fe(PA)_2$" plus 1.8 mM HOOH, (c) 3.5 mM "$Fe(PA)_2$" plus 7 mM HOOH, and (d) solution c after 23 h [scan rate 0.1 V s^{-1}; GCE (area, 0.09 cm^2)].

(2:1 mole ratio) that contains O_2 (1 atm) exhibits a reversible couple at +0.18 V vs SCE (analogous to that of Figure 4C) as well as a large irreversible peak for O_2 at −0.8 V vs SCE. Controlled-potential electrolysis (−0.6 V vs SCE) of this solution causes the solution to decolorize and yields a product solution whose voltammogram includes the couple at +0.18 V and two anodic peaks (a small peak at +1.0 V and a large peak at +1.25 V). After 1 h the peak at +1.25 V has decreased in size while that at +1.00 has grown, to give a cyclic voltammogram that is identical with that in Figure 4C. Controlled-potential electrolysis of this $Fe(PA)_2/O_2$ system in the presence of 1 M cyclohexane yields cyclohexanone with 49% efficiency ($4e^-$/ketone).

(b) Kinetic Measurements. In py/HOAc solvent the $Fe^{II}(DPAH)_2$ complex has the same absorption band (λ_{max}) as Fe^{II}(DPA), but its molar absorptivity is greater. Addition of more $DPAH^-$ does not affect the absorbance.

The reaction kinetics for the oxidation of $Fe^{II}(PA)_2$ and $Fe^{II}(DPAH)_2$ by HOOH and O_2 in py/HOAc solvent have been monitored by UV−visible spectrophotometry. The apparent reaction orders and rate constants have been determined from the initial rates of disappearance for $Fe^{II}(PA)_2$ and $Fe^{II}(DPAH)_2$ [λ_{max} 402 nm (ϵ 2000 cm^{-1} M^{-1}) and λ_{max} 394 nm (ϵ 2700 cm^{-1} M^{-1}), respectively]. The rates of reduction of $(DPAH)_2Fe^{III}OFe^{III}(DPAH)_2$ to $Fe^{II}(DPAH)_2$ have been determined via the latter's rate of formation.

The second-order rate constant is (2 ● 1) × 10^3 M^{-1} s^{-1} for the 1:1 combination of $Fe(PA)_2$/HOOH in py/HOAc but decreases to (2 ± 1) × 10^2 M^{-1} s^{-1} when the $Fe(PA)_2$/HOOH ratio is 1:200. In dimethylformamide the combination of two $Fe(PA)_2$ molecules with one HOOH results in the stoichiometric formation

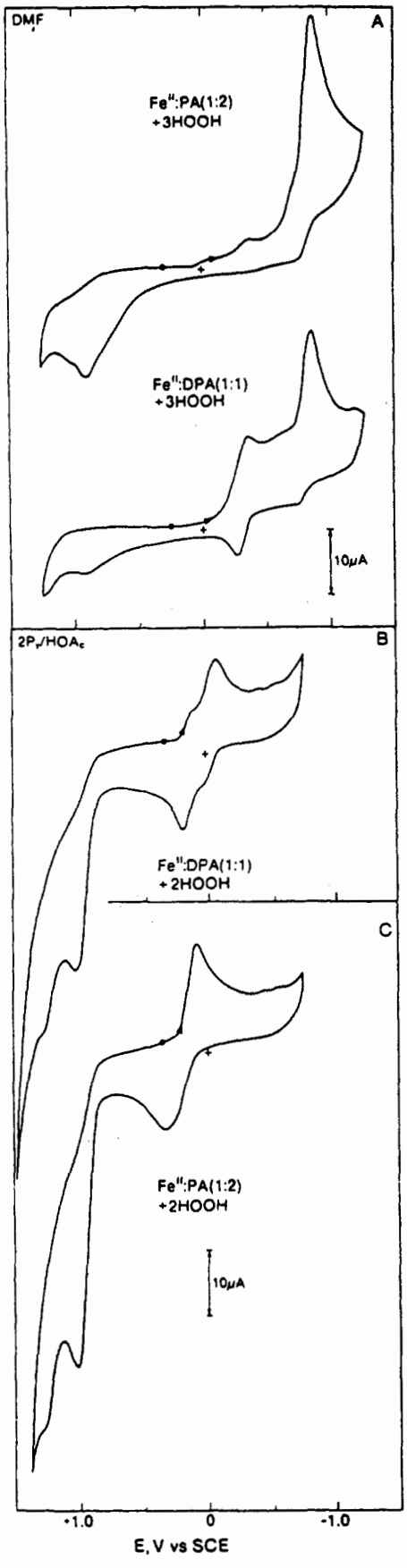

Figure 4. Cyclic voltammograms of (A) 2 mM Fe^{II}/PA (1:2) plus 6 mM HOOH and 2 mM Fe^{II}/DPA (1:1) plus 6 mM HOOH in DMF (0.1 M TEAP), (B) 2 mM Fe^{II}/DPA (1:1) plus 4 mM HOOH in 2:1 py/HOAc (0.1 M TEAP), and (C) 2 mM Fe^{II}/PA (1:2) plus 4 mM HOOH in 2:1 py/HOAc (0.1 M TEAP) [scan rate 0.1 V s^{-1}; GCE (area 0.09 cm^2)].

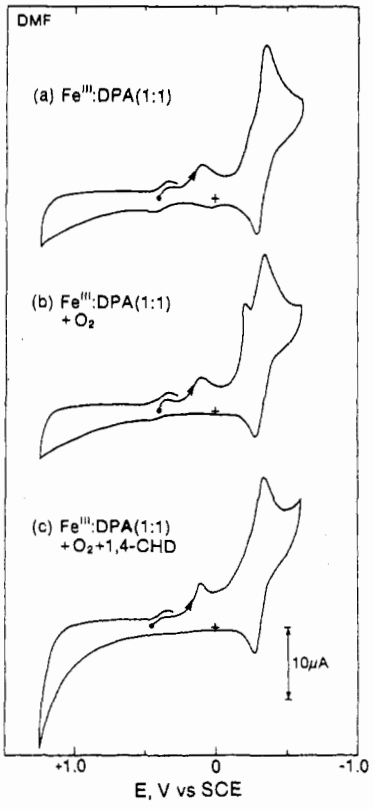

Figure 5. Cyclic voltammograms in DMF (0.1 M TEAP) of (a) Fe^{III}/DPA (1:1), (b) 2 mM Fe^{III}/DPA (1:1) plus O_2 (1 atm), and (c) Fe^{III}/DPA (1:1) plus O_2 (1 atm) plus 1 M 1,4-CHD [scan rate 0.1 V s^{-1}; GCE (area 0.09 cm^2)].

of $[(PA)_2Fe(OH)]_2$; the second-order rate constant is 2.5×10^3 M^{-1} s^{-1}. Likewise, $Fe^{II}(DPAH)_2$ is oxidized by HOOH; the rate constant is $(5 \pm 1) \times 10^3$ M^{-1} s^{-1}.

In contrast to $Fe(PA)_2$, which in py/HOAc solvent is resistant toward dioxygen, $Fe^{II}(DPAH)_2$ is rapidly autoxidized to $(DPAH)_2FeOFe(DPAH)_2$. The reaction order with respect to $Fe^{II}(DPAH)_2$ and dioxygen is unity for each, but 4 mol of $Fe^{II}(DPAH)_2$ is consumed/mol of dioxygen. This stoichiometry has been confirmed from the change in the concentration of the $Fe^{II}(DPAH)_2$ complex in solutions with limiting amounts of dioxygen. The apparent second-order rate constant, k_{ox}, has a value of 1.3 ± 0.5 M^{-1} s^{-1} ($k_{obs}/4$).

The oxidized product $[(DPAH)_2Fe^{III}OFe^{III}(DPAH)_2]$, which does not exhibit any absorption bands in the 300–800-nm region, is rapidly reduced to $Fe^{II}(DPAH)_2$ by PhNHNHPh, H_2NNH_2, $PhCH_2SH$, and H_2S ($k_{red} = 6.5 \pm 0.5$, 0.6 ± 0.3, 0.5 ± 0.3, and 2.8 ± 0.5 M^{-1} s^{-1}, respectively) to give PhN=NPh, N_2, $PhCH_2SSCH_2Ph$, and elemental sulfur (S_8), respectively.

Reduction of $Fe(DPA)^+$ in the Presence of Dioxygen. Figure 5 illustrates the cyclic voltammograms for the reduction of $Fe^{III}(DPA)^+$ in the absence and presence of dioxygen, which are similar to that for Fe(DPA) (Figure 1B), except the relative peak heights are different. In the presence of dioxygen there is an enhancement of the −0.35-V reduction peak, suppression of the −0.28- and +0.05-V reverse-scan oxidation peaks, and the appearance of a new reduction peak at −0.22 V. The latter splits into two overlapped reduction peaks (−0.15 and −0.22 V) when the scan rate is reduced to 0.036 V s^{-1}. In the presence of a 500-fold excess of 1,4-cyclohexadiene (1,4-CHD) (Figure 5), these new reduction peaks are totally suppressed.

The $Fe^{III}(DPA)^+/O_2$ system has been further characterized by a voltammetric ring–disk experiment, which is illustrated by the curves of Figure 6. The disk electrode is scanned from the rest potential (+0.42 V) to −1.0 V with the potential of the ring electrode at +0.25 V. In the absence of dioxygen (solid line) the upper curve gives the reduction current at the disk electrode for $Fe(DPA)^+$ and the lower solid line indicates the ring-electrode

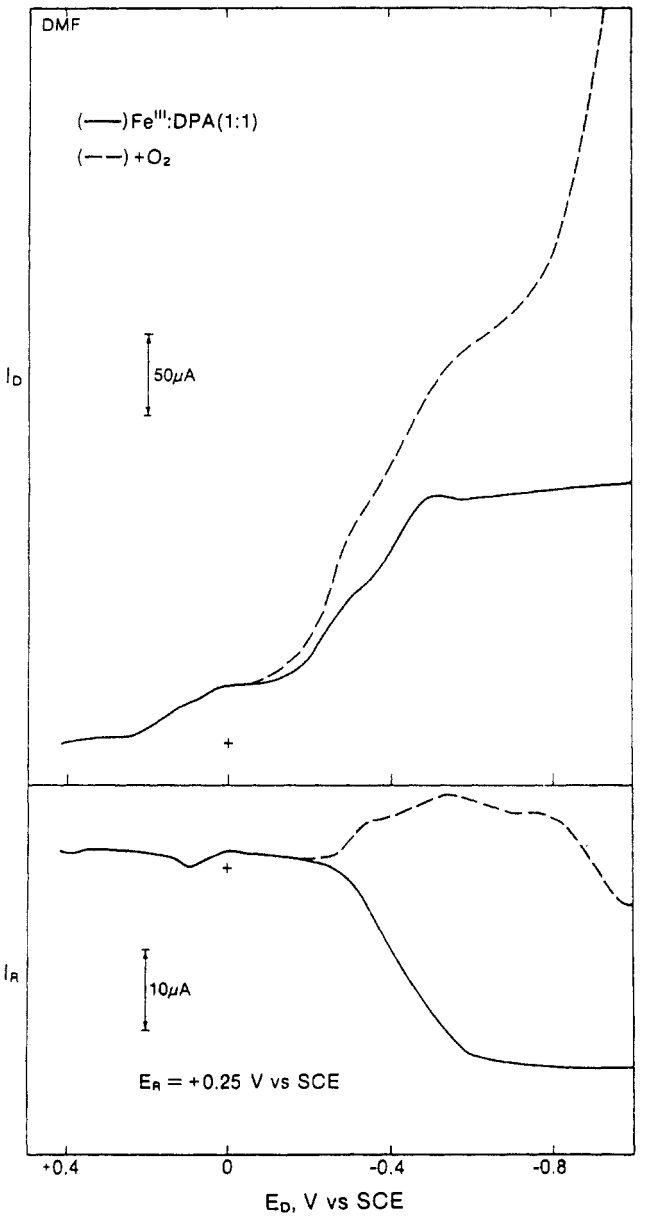

Figure 6. Voltammetric reduction of 2 mM Fe^{III}/DPA (1:1) in DMF (0.1 M TEAP) in the absence and presence of O_2 (1 atm) at a rotated GC disk electrode (400 rpm) and the electrochemistry of its reduction products at a GC ring electrode at +0.25 V vs SCE.

current for the reoxidation at +0.25 V of the product species from the disk electrode [Fe^{II}(DPA)]. The experimental collection efficiency (I_R/I_D) at the current plateaus of Figure 6 is 0.15, which is much smaller than the theoretical value of 0.42 for the electrode. In the presence of dioxygen (dotted line) the disk current is enhanced for disk potentials more negative than −0.02 V. The ring current with O_2 does not change until the disk potential is more negative than−0.20 V. When the disk-electrode potential is −0.6 V, the ring electrode exhibits a reductive current at +0.25 V rather than the oxidative current when O_2 is absent. This reductive current has a half-wave potential of +0.4 V vs SCE. For disk potentials more negative than −0.90 V, the ring current becomes anodic again (due to the oxidation of $O_2^{\bullet-}$ from the reduction of O_2 at the disk electrode).

Discussion and Conclusions

The cyclic voltammograms for the Fe^{II}/PA system indicate that only the 1:3 ratio results in a reversible couple (Figure 1A and Table I) with both species stable in solution. However, for Fe(PA)$_2$ the cyclic voltammogram is more complex with evidence for some Fe(PA)$_3^-$ (a small anodic peak at 0.00 V in Figure 1A). Oxidation

Scheme I

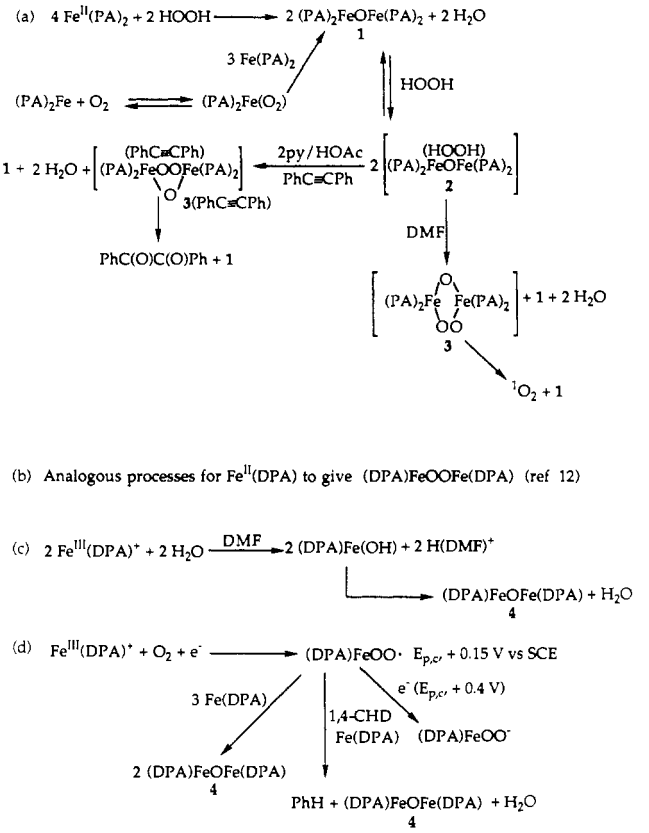

of Fe(PA)$_2$ appears to involve residual water to give Fe(PA)$_2$(OH) (Table I).

The Fe^{II}/DPA system forms a stable Fe(DPA)$_2^{2-}$ complex with a reversible redox couple (Figure 1B and Table I). With a 1:1 Fe:DPA mole ratio the cyclic voltammogram indicates that several species are present (Figure 1B) with the most positive couple characteristic of the solvated iron(II) ion (Table I). With a reverse scan there is a broad reduction peak at −0.30 V that confirms the presence of Fe(DPA)$_2^-$ in combination with another species that is reduced at a slightly less negative potential [probably Fe(DPA)(DPAH)]. Thus, Fe(DPA) undergoes a solvent-induced equilibration.

$$2\text{Fe(DPA)} + n\text{DMF} \rightleftarrows \text{Fe(DPA)}_2^{2-} + \text{Fe(DMF)}_n^{2+} \quad (1)$$

The addition of HOOH to solutions of Fe^{II}(PA)$_2$ and Fe^{II}(DPA) causes the iron complexes to be oxidized and results in product species with completely new electrochemistry (Figure 1). When DMF solutions of Fe(PA)$_2$ and Fe(DPA) are saturated with O_2 (1 atm), Fe(PA)$_2$ (slowly) and Fe(DPA) (rapidly) are transformed to species that have electrochemistries similar to those of the Fe(PA)$_2$/HOOH and Fe(DPA)/HOOH systems (Figure 2). With both oxidations (HOOH and O_2), the reductive current is half that for the oxidation of Fe(PA)$_2$ and Fe(DPA) (prior to the addition of HOOH or O_2). The electrochemistry and spectroscopy for these product solutions are essentially the same as those for (PA)$_2$FeOFe(PA)$_2$ and (DPA)FeOFe(DPA) (Table I). The reactions associated with these transformations are outlined in Scheme I.

When excess HOOH is added to Fe(PA)$_2$ or Fe(DPA) in DMF, it is rapidly decomposed to dioxygen (Figure 4). In a related study the evolved dioxygen has been shown to be in the singlet state.[12] This reaction sequence is outlined in Scheme Ia.

The electrochemical results of Figure 4A indicate that the HOOH adduct of (DPA)FeOFe(DPA) is less stable than that of (PA)$_2$FeOFe(PA)$_2$ (species **2** of Scheme I), which is consistent with the more rapid decomposition of HOOH in the presence of (DPA)FeOFe(DPA). In the pyridine/acetic acid (2:1 mole ratio) solvent system, addition of excess HOOH to (PA)$_2$FeOFe(PA)$_2$

or (DPA)FeOFe(DPA) does not result in O_2 evolution, but yields stable HOOH adducts (Figure 3 and 4). In contrast to free HOOH, which is oxidized at +1.25 V vs SCE, the adducts are oxidized at +1.00 V (Table I). In a recent investigation,[12] the $(PA)_2FeOFe(PA)_2$ and (DPA)FeOFe(DPA) complexes in a 2:1 py/HOAc solvent system have been shown to activate HOOH for the selective dioxygenation of PhC≡CPh to PhC(O)C(O)Ph and the direct transformation of cyclohexane to cyclohexanone (95%, with 5% c-$C_6H_{11}OH$). On the basis that (a) $^1O_2$ is evolved when $(PA)_2FeOFe(PA)_2$ and HOOH are combined in DMF, (b) $(PA)_2FeOFe(PA)_2$ and HOOH form a stable adduct (**2**, Scheme I) in 2:1 py/HOAc, and (c) in the presence of the latter system, PhC≡CPh undergoes dioxygenation, we conclude that there is a common reactive intermediate $[(PA)_2FeO(OO)Fe(PA)_2$ (**3**) (and (DPA)FeOOFe(DPA) for the (DPA)FeOFe(DPA)/HOOH system)].[12]

The reductions of $Fe^{III}(DPA)^+$ in the absence and presence of O_2, which are illustrated by the voltammograms of Figure 5 and the ring-disk current-voltage curves of Figure 6, indicate that an easily reduced intermediate is formed [probably (DPA)FeOO•; $E_{p,c}$ = +0.4 V vs SCE]. This potential is the same as that for the reduction of HOO• in DMF,[17] which is reasonable for electron addition to a peroxy radical formulation, (DPA)FeOO•. Scheme Ic outlines a self-consistent reaction sequence for the hydrolytic dimerization of $Fe^{III}(DPA)^+$, and Scheme Id outlines the reaction intermediates when O_2 is present. With excess $Fe^{II}(DPA)$ present, the (DPA)FeOO• intermediate is immediately transformed to (DPA)FeOFe(DPA) (**4**). If excess 1,4-cyclohexadiene (1,4-CHD) is present, the peak at −0.22 V (Figure 5) is not observed because the (DPA)FeOO• intermediate reacts with the allyl hydrogen atoms of 1,4-CHD.

In pyridine/acetic acid solvent, $Fe^{II}(DPAH)_2$ in the presence of O_2 and excess substrate is autoxidized to a reactive intermediate, which ketonizes methylene carbons and dioxygenates acetylenes, aryl olefins, and catechols.[14] Because the products are identical with those that result from the reactive intermediate formed from the combination of (DPA)FeOFe(DPA) and excess HOOH, (DPA)FeOOFe(DPA),[12] the dioxygenation of the substrates must result from a similar reactive intermediate. The close parallels of the product profiles as well as the results of the kinetic measurements prompt the conclusion that the combination of $Fe^{II}(DPA)_2$ and O_2 results in the initial formation of the reactive intermediate $(DPAH)_2FeOOFe(DPAH)_2$ via a rate-limiting step. In the absence of substrate, the active catalyst is rapidly autoxidized to $(DPAH)_2FeOFe(DPAH)_2$, which is reduced to $Fe^{II}(DPAH)_2$ by PhNHNHPh, H_2NNH_2, $PhCH_2SH$, and H_2S.

A related binuclear complex,[18] $[(Ph_3PO)_4FeOOFe(OPPh_3)_4](ClO_4)_4$, also selectively dioxygenates PhC≡CPh and ketonizes methylene carbons.[12] With $(PA)_2FeOFe(PA)_2$·HOOH (**2**) the presence of substrate appears to be necessary to induce formation of the reactive intermediate complex [**3**(PhC≡CPh)].

Acknowledgment. This work was supported by the National Science Foundation under Grant No. CHE-8516247 (D.T.S.) and with a Graduate Fellowship (S.A.R.). We are grateful (a) to the U.S. Air Force Institute of Technology Civilian Institute Program for the award of a Fellowship to S.A.R. and (b) to the Universidad Catolicade Chile for a Research Leave to P.C.

(17) Cofré, P.; Sawyer, D. T. *Inorg. Chem.* **1986**, *25*, 2089-2092.

(18) Sawyer, D. T.; McDowell, M. S.; Spencer, L.; Tsang, P. K. S. *Inorg. Chem.* **1989**, *28*, 1166.

Contribution from the Department of Chemistry, The Pennsylvania State University, University Park, Pennsylvania 16802, and The Contrast Media Research Department, Squibb Institute for Medical Research, P.O. Box 191, New Brunswick, New Jersey 08903

Laser-Induced Europium(III) Luminescence and NMR Spectroscopic Characterization of Macrocyclic Diaza Crown Ether Complexes Containing Carboxylate Ligating Groups

Richard C. Holz,† Scott L. Klakamp,† C. Allen Chang,‡ and William DeW. Horrocks, Jr.*,†

Received October 3, 1989

The Eu^{3+} and Y^{3+} complexes of 1,10-diaza-4,7,13,16-tetraoxacyclooctadecane-*N*,*N*′-diacetic acid (K22DA), 1,7-diaza-4,10,13-trioxacyclopentadecane-*N*,*N*′-diacetic acid (K21DA), and the open-chain analogue ethylene glycol bis(β-aminoethyl ether)-*N*,*N*,*N*′,*N*′-tetraacetic acid (EGTA) have been characterized in solution by using Eu^{3+} laser-induced luminescence and ^1H and ^{13}C NMR spectroscopy. All of these ligands form 1:1 complexes with Eu^{3+} in solution with the luminescence lifetimes in H_2O and D_2O providing the number of coordinated water molecules. Stepwise changes in the coordination environment of the Eu^{3+} and Y^{3+} ions were monitored spectroscopically for each complex as a function of temperature. In addition, the Eu^{3+} spectral changes as a function of pH were examined. These results indicate that Eu^{3+} and Y^{3+} each coordinate all the ligating atoms of K21DA but that K22DA undergoes fluctional processes, suggesting that the macrocyclic cavity size is too large to accommodate the metal ion properly. The noncyclic EGTA ligand, by comparison, appears to undergo an equilibrium process of wrapping and unwrapping at room temperature. The luminescence and NMR results demonstrate the importance of a proper match between metal ion size and macrocyclic cavity size.

Introduction

Metal complexation by mixed aza and oxa macrocyclic ligands with or without coordinating pendant arms has recently received considerable attention. If certain features are "built" into these macrocyclic ligands, such as ligand charge density and/or macrocyclic cavity size, they can be designed to accommodate specific metal ions or groups of metal ions.[1,2] These macrocyclic ligands have many potential uses including synthetic ionophores, models of protein metal binding sites, NMR imaging agents, sequestering agents, and metal ion separation reagents. Specifically, we are interested in two macrocyclic aminocarboxylic acids that have binding selectivity toward the lanthanide ions in general and, within this series, toward individual lanthanide ions.[3-5] These two ligands, 1,10-diaza-4,7,13,16-tetraoxacyclooctadecane-*N*,*N*′-diacetic acid

†The Pennsylvania State University.
‡Squibb Institute for Medical Research.

(1) Lehn, J.-M. *Acc. Chem. Res.* **1978**, *11*, 49.
(2) Christensen, J. J.; Eatough, D. J.; Izatt, R. M. *Chem. Rev.* **1974**, *74*, 351.
(3) Chang, C. A.; Rowland, M. E. *Inorg. Chem.* **1983**, *22*, 3866.
(4) Chang, C. A.; Ochaya, V. O.; Sekhar, V. C. *J. Chem. Soc., Chem. Commun.* **1985**, 1724.
(5) Chang, C. A.; Ochaya, V. O. *Inorg. Chem.* **1986**, *25*, 355.

0020-1669/90/1329-2651$02.50/0